Ocean Acoustic Propagation: Fluctuations and Coherence in Dynamically Active Shallow-Water Regions

Timothy F. Duda
Applied Ocean Physics and Engineering Department, MS 11
Woods Hole Oceanographic Institution, Woods Hole, MA 02543
phone: (508) 289-2495 fax: (508) 457-2194 email: tduda@whoi.edu

Grant Number: N00014-05-1-0482
http://www.whoi.edu/science/AOPE/cofdl/timdcv.html

LONG TERM GOALS

The goals are to understand the nature and the causes of acoustic signal fluctuations in the shallow water environment (i.e. the physical mechanisms). This knowledge may allow better prediction of acoustic system performance and more successful exploitation of acoustic signal properties. Here, signal means any identifiable acoustic reception, including noise of unknown origin, identifiable signals from discrete sources, and intentional signals.

OBJECTIVES

An objective is to gain understanding of the fluctuation behavior of fully three-dimensional acoustical propagation (including horizontal deflection from seafloor and water column heterogeneities) in shallow-water environments with three-dimensional structure at all significant scales. This will allow evaluation of the validity of commonly used two-dimensional approximations for ocean structures and propagation physics. A second objective is to classify acoustic stability and fluctuation using signal parameters. We are also investigating the time scales over which the often-invoked assumption of stationarity is valid.

APPROACH

To understand and predict shallow-water acoustic conditions, including examination of the influences of assorted three-dimensional shallow-water oceanic features on acoustic propagation, we have been analyzing experimental data and implementing acoustic propagation modeling and theory. This year's effort is aimed primarily at summer conditions in the temperate ocean, but also includes conditions found just inshore of shelfbreak fronts, such as the one in the Mid-Atlantic Bight where there is warm offshore water and winter-cooled water on the shelf. In the frontal situation there may be a thin deep layer capped by a deep thermocline on the near-edge section of the shelf. These are stratified regimes which support internal waves and are downward refracting acoustically. Observations show that packets of nonlinear mode-one internal gravity waves often dominate in this situation. These internal waves have various effects which are the subject of our research. Such waves at the location of a sound source would control acoustic mode excitation, and thus the effects of mode-stripping on long propagation paths. Such waves along a sound propagation path can cause mode coupling, altering mode-stripping effects at further range. Long internal waves or internal tides (having wavelengths tens of kilometers) can alter mode shapes and mode stripping, and can alter source excitation, but probably do not cause mode coupling.

Report Documentation Page

Form Approved
OMB No. 0704-0188

1. REPORT DATE	2. REPORT TYPE	3. DATES COVERED
30 SEP 2008	**Annual**	**00-00-2008 to 00-00-2008**

4. TITLE AND SUBTITLE	5a. CONTRACT NUMBER
Ocean Acoustic Propagation: Fluctuations And Coherence In Dynamically Active Shallow-Water Regions	5b. GRANT NUMBER
	5c. PROGRAM ELEMENT NUMBER
6. AUTHOR(S)	5d. PROJECT NUMBER
	5e. TASK NUMBER
	5f. WORK UNIT NUMBER
7. PERFORMING ORGANIZATION NAME(S) AND ADDRESS(ES) **Woods Hole Oceanographic Institution,Applied Ocean Physics and Engineering Department, MS 11,Woods Hole,MA,02543**	8. PERFORMING ORGANIZATION REPORT NUMBER
9. SPONSORING/MONITORING AGENCY NAME(S) AND ADDRESS(ES)	10. SPONSOR/MONITOR'S ACRONYM(S)
	11. SPONSOR/MONITOR'S REPORT NUMBER(S)

12. DISTRIBUTION/AVAILABILITY STATEMENT
Approved for public release; distribution unlimited

13. SUPPLEMENTARY NOTES
code 1 only

14. ABSTRACT
The goals are to understand the nature and the causes of acoustic signal fluctuations in the shallow water environment (i.e. the physical mechanisms). This knowledge may allow better prediction of acoustic system performance and more successful exploitation of acoustic signal properties. Here, signal means any identifiable acoustic reception, including noise of unknown origin, identifiable signals from discrete sources, and intentional signals.

15. SUBJECT TERMS

16. SECURITY CLASSIFICATION OF:			17. LIMITATION OF ABSTRACT	18. NUMBER OF PAGES	19a. NAME OF RESPONSIBLE PERSON
a. REPORT	b. ABSTRACT	c. THIS PAGE			
unclassified	**unclassified**	**unclassified**	**Same as Report (SAR)**	**14**	

We are comparing our theoretically based ideas and computationally-derived results with ground-truth field observations from three experiments. One is the ONR ASIAEX South China Sea study, This study yielded four papers in the October 2004 *IEEE Journal of Oceanic Engineering* containing analysis of acoustic signals at 250-450 Hz from sources at ranges of 21 and 32 kilometers: Orr et al. [2004], Mignerey and Orr [2004], Chiu *et al*. [2004], and Duda *et al*. [2004]. The year 2006 report on this project describes those results. The next experiment is the Littoral Environmental Acoustics Research (LEAR) portion of the ONR Shallow-Water 2006 experiment (SW06). This experiment was on the shelf in the Mid-Atlantic Bight east of New Jersey, and took place July-September 2006 [Tang *et al*., 2007]. The third experiment is the spring 2007 ONR/Taiwan NLIWI acoustics experiment in the ASIAEX area of the South China Sea [Reeder *et al*., 2008].

Because the data show strong signatures of horizontal refraction, we have moved more heavily this year into 3-D parabolic equation (PE) computational acoustic modeling. This tool is essential in sloped environments and where high lateral sound-speed gradients are found (such as in nonlinear internal waves, where the modal refractive has been observed to vary up to one-half percent, and acoustic mode critical angles can exceed five degrees [Reeder *et al*., 2008]). This tool builds on our 2-D PE capability which is based on a modified version of the RAM code (Mike Collins, NRL). The faster 2-D computations are best when refraction is absent, as they can include more complicated seafloor types.

The goal of the classification work is to identify unique shallow-water fluctuation regimes, classified in terms of fluctuation parameter state vectors received by an array, and relate them to their causes (large internal waves, small internal waves, focusing by alignment with internal wave crests, etc.). The ability to classify the propagation domain (i.e. identify the cause of dominating fluctuations) would enable modeling, prediction, and extrapolation. This would be a through-the-sensor classification or inversion technique. A specific objective is a multi-parameter definition of signal characteristics which allows description of the fluctuations in terms of physical conditions, which would serve to condense the complicated effects of moving internals wave (and/or fronts) into meaningful and potentially predictable measures of acoustic signal parameters. At this time, a data clustering (cluster analysis) approach is being examined.

WORK COMPLETED

A large number of LEAR/SW06 pulses transmitted from moored sources to the WHOI L-array (co-located HLA/VLA) were analyzed this year. Figure 1 shows the experimental arrangement. Figures 2-4 show coherence length estimates obtained from analysis of HLA signals after array shape correction and beam steering. Phases of fully dispersed 100-Hz mode-1 pulse arrivals were used to obtain the array shape, using an ensemble averaging technique to reduce effects of noise and pulse variation. The array was dragged into a new shape twice during the study, with at least one instance being caused by nonlinear internal waves. The figures show that sound arrival angle is altered and coherence length is diminished by the presence of internal waves between the source and receiver. The coherence length at fixed steering angle fluctuates greatly because of sound refraction and waveform interference. The time series of maximum observed coherence length is more regular and reaches very long lengths because refraction is adaptively corrected for, but the maximum coherence length is not always long, with low values at times of wave activity. The coherence is governed by phase fluctuations along the length of the array, with amplitude fluctuations taking a secondary role. The processing method is effectively broadband because entire pulse arrival time series at each phone are correlated against each other to achieve the result. The analysis methods work best at high signal to noise ratio.

This year a paper was published explaining a new method of L-array processing to divulge azimuthally-dependent shallow-water pulse propagation (Collis *et al.,* 2008). The method utilizes both HLA and VLA signals and compares the coherence length of an azimuthal mode interference pattern with the observed coherence. Two different coherence length regimes were found for one source at one steering angle. Figure 5 shows an interpretation of the results. The curves show hypothetical coherence versus beam steering angle from broadside, which would require a larger experiment to measure. (Again, we only have simultaneous measurements at one angle, 28 degrees.) Many pulses are required to effectively measure the coherence angle, and the time series is crucial for interpreting the causes of the behavior, so analysis of a few towed-source pulses transmitted to the L-array from other directions by other SW06 PI's would not be helpful in building up the full curves.

This year, the 3-D parabolic equation (PE) code has been used extensively. Application was to the 2007 South China Sea experiment. Figure 6 shows the experiment region. At this time we are not using the code in a mode that allows the density of the seafloor to differ from that of the water. Adjustment of the code to allow this, using methods of Tappert and Smith, has been implemented in a test mode, but slows the code by 50% (a second parallel field computation is made), so it is not used routinely. The code and initial results obtained with it appear in a WHOI report issued in December, 2006. WHOI postdoc Y.-T. Lin has also been working with the code and has modified it to allow variable depth. Some forward-looking modeling of a canyon site north or Taiwan where the ONR Quantifying, Predicting and Exploiting Uncertainty (QPE) program is focused.

The conditions measured by the 2007 South China Sea PI's were used to model sound propagation, Figures 7 and 8. The results show promising agreement with measurements [Reeder *et al.,* 2008]. The simulations mimic the propagation directly down the waves (or close to it), which is what was observed. The simulations provide results at many other angles, where other degrees of focus may occur.

RESULTS

Sound refraction effects measured at the South China Sea site were found to be consistent with model results and published in an Ocean meeting paper [Reeder *et al*., 2008]. The paper reports mode refractive indices and critical angles of the internal waves present during the experiment. The 3D acoustic effects were replicated with a model. The good comparison between the experiment and the model output suggests that behavior at source-receiver geometries other than that of the experiment (down the internal wave duct, Figure 6) can be examined. Also, propagation through commonly-observed curved internal waves can be studied. In this situation, critical mode refraction effects evolve as the sound moves along the curved duct, rather than being constant. As a result, the internal waves may behave like prisms, separating modes.

An examination of propagation down an internal wave duct that fades away, as was observed a few times in SW06, was performed in collaboration with Y.-T. Lin of WHOI. This was presented at the summer 2008 Acoustical Society meeting and a paper in being written. The results show that a highly time-dependent mix of acoustic mode beams can emerge from the duct, with the beams of each mode appearing to be independent.

Time series of internal tides and nonlinear internal wave packets were measured at many SW06 moorings. These each propagate (often in the same direction) at speeds of 0.7 to 0.8 m/s. The internal tides have wavelength of 25 to 40 km, whereas the nonlinear waves have 300 to 1200 m wavelengths.

Using the time series to construct a realistic temporally evolving vertical slice of sound speed (similar to Chui *et al*. 2004), time-varying signal level vs. range curves can be generated (Figure 3). At 9 km range, depth-averaged signals can vary by 6 dB (depth averaging quantifies seafloor loss effects), with range-averaged single-depth arrivals being even more variable. The effects of varying mode excitation by the fixed-depth source, as well as that of varying mode attenuation parameters, are being examined for relative importance.

Finally, a paper was published showing horizontal array gain and coherence length variability for along-internal wave duct propagation in SW06 [Collis *et al.*, 2008]. The paper showed results for one acoustic frequency (100 Hz) along one path using a few hours of data. Coherence scale estimates for weak internal-wave periods were about 75 m (5 wavelengths). For string internal-wave periods they were about 220 m (15 wavelengths). This year, new results are available for many weeks of pulse data for three frequencies along the 30-degree path (Figure 1) and two frequencies along the 300-degree path. Figures 2, 3 and 4 shows some results in graphical form. Tabulating the results and comparison with theoretically-developed predictions is underway at this time.

IMPACT/APPLICATIONS

The results may be useful in the signal processing domain. Algorithms may be developed that are robust to signal fluctuations, or which may exploit them. For example, processing might exploit fluctuations by utilizing intermittent but strong signal peaks, or predicting time limits for coherent analysis, or predicting wait intervals before signals are reacquired after fade-outs.

RELATED PROJECTS

At this time the PI is a participant in the LEAR portion of SW06, and is currently processing and examining the data from the order-50 moorings that collected water-column variability in the area of the acoustic experiments. We are working with D. Knobles (ARL-UT), Jon Collis (Colorado School of Mines) and H. DeFerrari (Miami) to examine the environment during their propagation experiments, and with J. Lynch (WHOI) and M. Badiey (U Del.). The ONR postdoctoral awardees Y.-T. Lin (WHOI) and Jon Collis (Boston University) worked this year with the PI this year on 2-D and 3-D simulations and on LEAR/SW06 data analysis. The PI is working with NLIWI ONR Physical Oceanography PI's analyzing data from the SW06 and 2007 South China Sea, and QPE experiment sites. This year Ilya Udovydchenkov joined the PI as an ONR postdoctoral fellow working on coupled-mode long-distance deep-water acoustics.

REFERENCES

Chiu, C.-S., S. R. Ramp, C. W. Miller, J. F. Lynch, T. F. Duda, and T. Y. Tang, Acoustic intensity fluctuations induced by South China Sea internal tides and solitons, *IEEE J. Oceanic Eng., 29,* 1249-1263, 2004.

Duda, T. F., J. F. Lynch, A. E. Newhall, L. Wu, and C.-S. Chiu, Fluctuation of 400-Hz sound intensity in the 2001 ASIAEX South China Sea Experiment, *IEEE J. Oceanic Eng., 29,* 1264-1279, 2004.

Mignerey, P. C. and M. H. Orr, Observations of matched-field autocorrelation time in the South China Sea, *IEEE J. Oceanic. Eng., 29,* 1280-1291, 2004.

Orr, M. H., B. H. Pasewark, S. N. Wolf, J. F. Lynch, T. Schroeder, and C. -S. Chiu, South China Sea internal tide/internal waves - Impact on the temporal variability of horizontal array gain at 276 Hz, *IEEE J. Oceanic. Eng., 29,* 1292-1307, 2004.

PUBLICATIONS

Duda, T. F., Temporal and cross-range coherence of sound traveling through shallow-water nonlinear internal wave packets, *J. Acoust. Soc. Am., 119,* 3717-3725, 2006. [published, refereed]

Duda, T. F., Initial results from a Cartesian three-dimensional parabolic equation acoustical propagation code, *WHOI Tech. Rept.,* WHOI-2006-041, 20 pages, Dec. 2006. [published, not refereed]

Duda, T. F., B. M. Howe and B. D. Cornuelle, Acoustic systems for global observatory studies, *MTS/IEEE Oceans '06 conference proceedings,* Boston, MA, 2006. [published, nor refereed]

Duda, T. F., A. K. Morozov, B. M. Howe, M. G. Brown, K. Speer, P. Lazarevich, P. F. Worcester, and B. D. Cornuelle, Evaluation of a long-range joint acoustic navigation/thermometry system, *MTS/IEEE Oceans '06 conference proceedings,* Boston, MA, 2006. [published, not refereed]

Heaney, K. D., G. Gawarkiewicz, T. F. Duda and P. F. J. Lermusiaux, Non-linear optimization of autonomous undersea vehicle sampling strategies for oceanographic data assimilation, *J. Field Robotics, 24,* 437-448, 2007. [published, refereed]

Newhall, A. E., T. F. Duda, K von der Heydt, J. D. irish, J. N. Kemp. S. A. Lerner, S. P. Liberatore, Y.-T. Lin, J. F. Lynch, A. R. Maffei, A. K. Morozov, A. Shmelev, C. J. Sellers, W. E. Witzell, Acoustic and oceanographic observations and configuration information for the WHOI moorings from the SW06 experiment, *Woods Hole Oceanog. Inst. Tech. Rept.,* WHOI-2007-04, June 2007. [published, not refereed]

Duda, T. F., B. M. Howe and J. H. Miller, Acoustics in global process ocean observatories, *Sea Technology, 48,* 35-38, 2007. [published, not refereed]

Duda, T. F., Examining the validity of approximations to fully three-dimendsional shallow-water acoustic propagation through nonlinear internal gravity waves, *IEEE Oceans '07 Aberdeen Conference proceedings,* June 2007. [published, not refereed]

Duda, T. F. and J. Collis, Acoustic field coherence in four-dimensionally variable shallow-water environments: estimation using co-located horizontal and vertical line arrays, *Underwater Acoustic Measurement and Technology Conference Proceedings*, Crete, Greece, June 2007. (Invited paper) [published, not refereed]

Irish, J. D., J. F. Lynch, J. N. Kemp, T. F. Duda, and A. E. Newhall, Moored array for measuring internal solitary waves during Shallow Water 06, *MTS/IEEE Oceans '07 Vancouver Conference Proceedings,* 2007. [published, not refereed]

Tang, D. J., J.N. Moum, J.F. Lynch, P. Abbot, R. Chapman, P. Dahl, T. Duda, G. Gawarkiewicz, S. Glenn, J.A. Goff, H. Graber, J. Kemp, A. Maffei, J. Nash and A. Newhall, ShallowWater 2006: a joint acoustic propagation/nonlinear internal wave physics experiment, *Oceanography*, 20(4), 156-167, 2007. [published, refereed]

Reeder, D. B., T. F. Duda and B. Ma, Short-range acoustic propagation variability on a shelf area with strong nonlinear internal waves, *IEEE Oceans '08 Kobe Conference Proceedings*, April 2008. [published, not refereed].

Duda, T. F., and L. Rainville, Diurnal and semidiurnal internal tide energy flux at a continental slope in the South China Sea, *J. Geophys Res (C), 113*, C03025, doi:10.1029/2007JC004418, 2008. [published, refereed]

Duda, T. F. and A. D. Pierce, History of Environmental Acoustics, 1960's to 2000's, *MTS/IEEE Oceans '08 Quebec Conference Proceedings*, September 2008. [published, not refereed].

Collis, J. M., T. F. Duda, J. F. Lynch, and H. A. Deferrari, Observed limiting cases of horizontal field coherence and array performance in a time-varying internal wavefield, *J. Acoust. Soc. Am.*, *124*, EL97, 2008. [published, refereed]

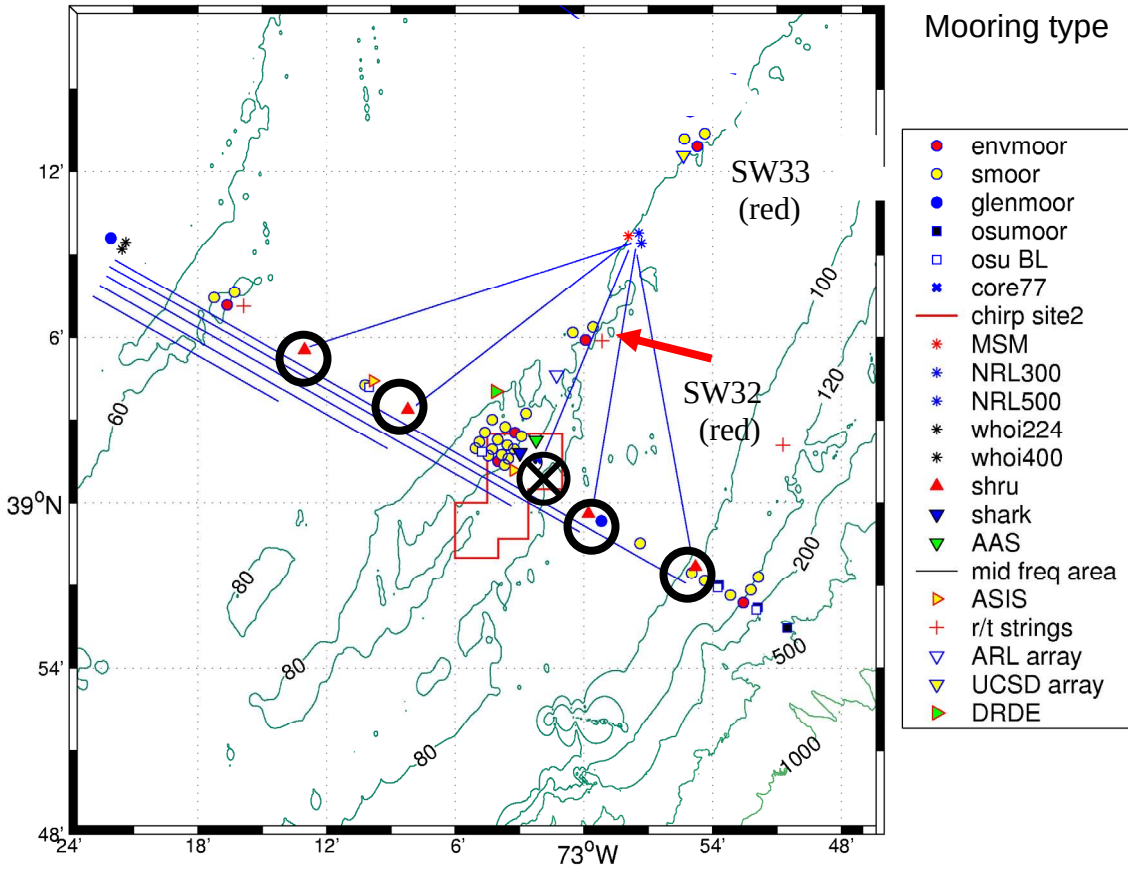

Figure 1. SW06 propagation paths from moored sources to moored receivers are shown with blue lines. The circles show single-phone SHRU receivers. The circle with the X shows the WHOI L-array (vertical line array (VLA) attached to horizontal line array (HLA) on the seafloor). The northwest site had 224 and 400 Hz sources. The northeast site had 100, 200, 300, 400, and 800 Hz sources. Environmental moorings SW33 and SW32 whose data are shown in Figs. 2 and 3 are marked. Data from mooring SW30 (not marked) near the L-array are also shown in the report. Depths contoured in meters.

[The L-array is near the center. At heading 30 (approx) are SW32 at 10 km distance, the northeast sources at 20 km, and SW33 at 25 km. The four SHRUS are near a line of heading 300, two offshore of the L-array and two inshore. The northwest sources are 32 km from the L-array along this line at about 60-m depth. The L-array and the 30-degrees line are at about 80-m depth.]

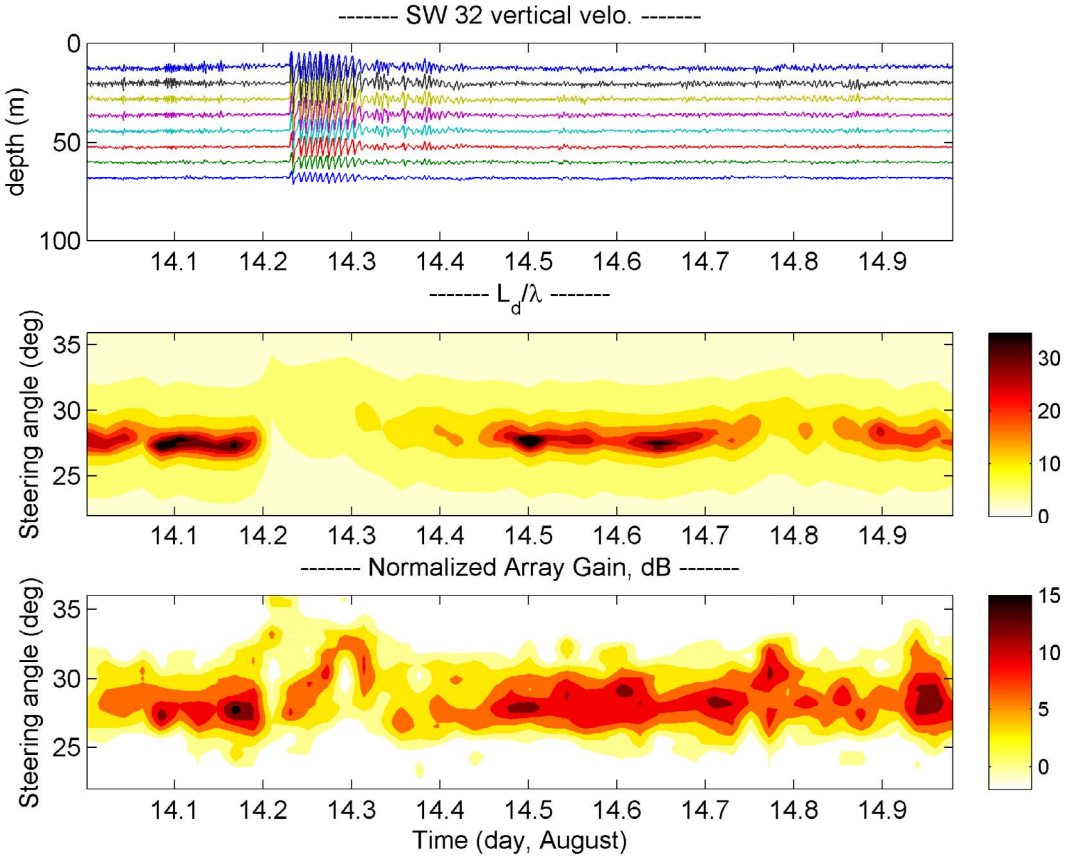

Figure 2. One-day long time series of derived quantities from 200-Hz pulses transmitted from the northeast site are show, along with internal waves measured along the path. (top) Vertical velocity at a few depths at site SW32). Velocity is scaled arbitrarily so that internal waves are visible. Time series for each depth are plotted so that zero value is located at the measurement bin depth. One packet of steep nonlinear waves is seen. (center) Contours of horizontal coherence length, normalized by acoustic wavelength, computed for pulses received along the HLA. Coherence length is computed as a function of time and beam steering angle. The maximum coherence length is reduced when the sound passes through the wave, whish is aligned such that sound travels along the crests. (bottom) The coherent-average signal power versus noise power (array gain) for the 32-element HLA is plotted as a function of beam steering angle and time. The sound is diverted by the waves and appears to arrive from a more easterly heading. The theoretical gain for a plane wave signal and incoherent noise is 10log(32) ~ 15 dB. High array gain is intermittently achieved. The angle at which array gain reaches maximum fluctuates. Gain is reduced during the internal wave event.

[(top) 14 large internal waves appear between day August 14.23 and 14.31. (center) The correlation length detected at steering angle 28 degrees is usually 20-30 wavelengths, decreasing from this peak at other angles. At the time of the waves the peak is at about 30 degrees and is reduced to about 5 wavelengths. (bottom) The array gain usually has a peak of 10 to 15 dB at steering angle 28 degrees. At the time of the waves there a two brief periods of peak gain less than 5 dB, occurring at rapidly variable angle.]

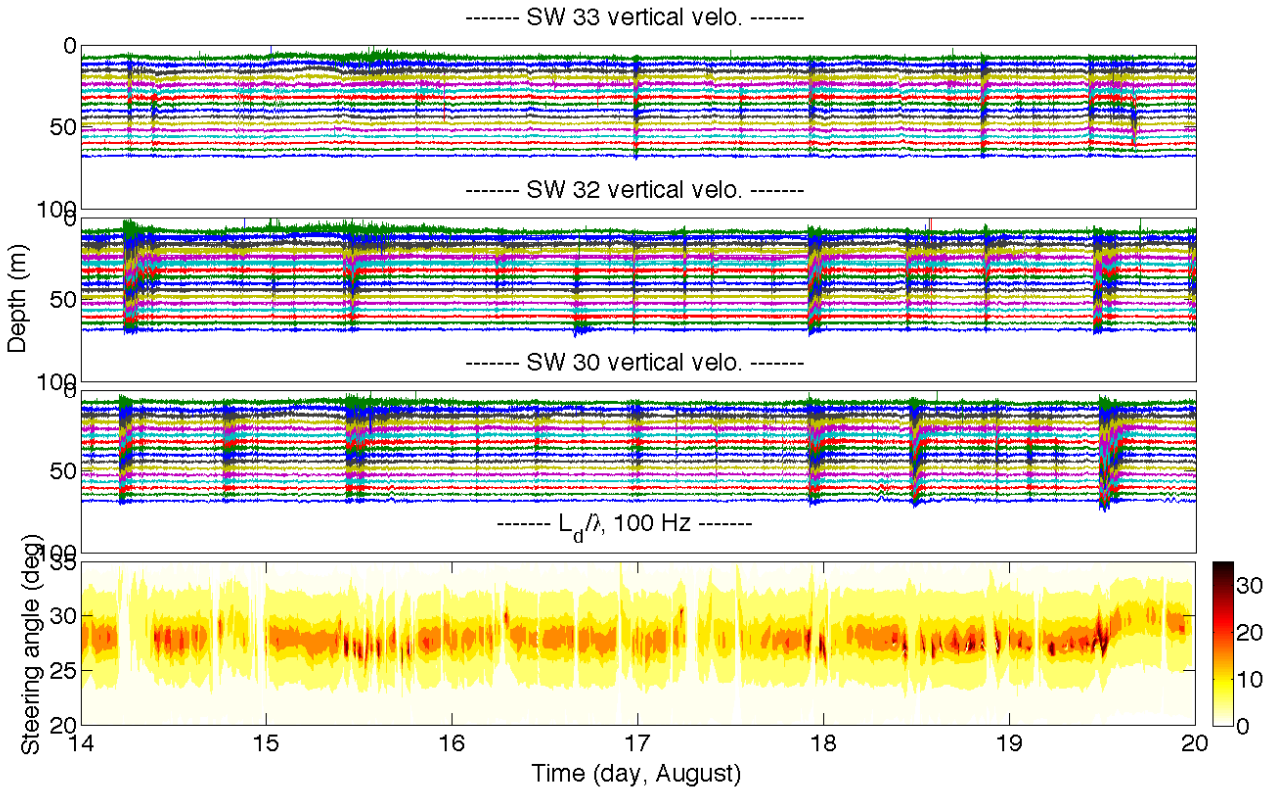

Figure 3. 100-Hz acoustic field horizontal coherence length estimates versus angle and time (six days) are contoured as in Figure 3. The top three panels show time series of vertical velocity, also as in Figure 3. In addition to SW32 velocity shown in Figure 3, velocity from SW33 to the northeast of the source is added, along with SW30 velocity measured near the L-array. Thus, moving down the figure, the wave timeseries progress from northeast to southwest along the propagation path. Some waves (eg. at August 18 noon, day 18.5) appear at the south only. (At other times the waves appear only at the north, not shown.) The lower panel shows the contour of time- and direction-dependent coherence length estimate. The maximum value of this fluctuates; the value at fixed angle fluctuates. The direction of maximum value fluctuates. The horizontal array is bent a fraction of a wavelength by internal waves just after 1030 UTC August 19, which alters the processing reuslts, which must include the array shape along the seafloor.

[Top three panels show eleven wave packets at SW32, about ten packets at SW30, and only about five packets at SW33 to the northeast. Thus, some of these wave packets, moving to the northwest, weaken at the northern (source) end of the line. The bottom panel shows periods of steady coherence behavior interrupted by rapidly varying behavior at the times of the waves.]

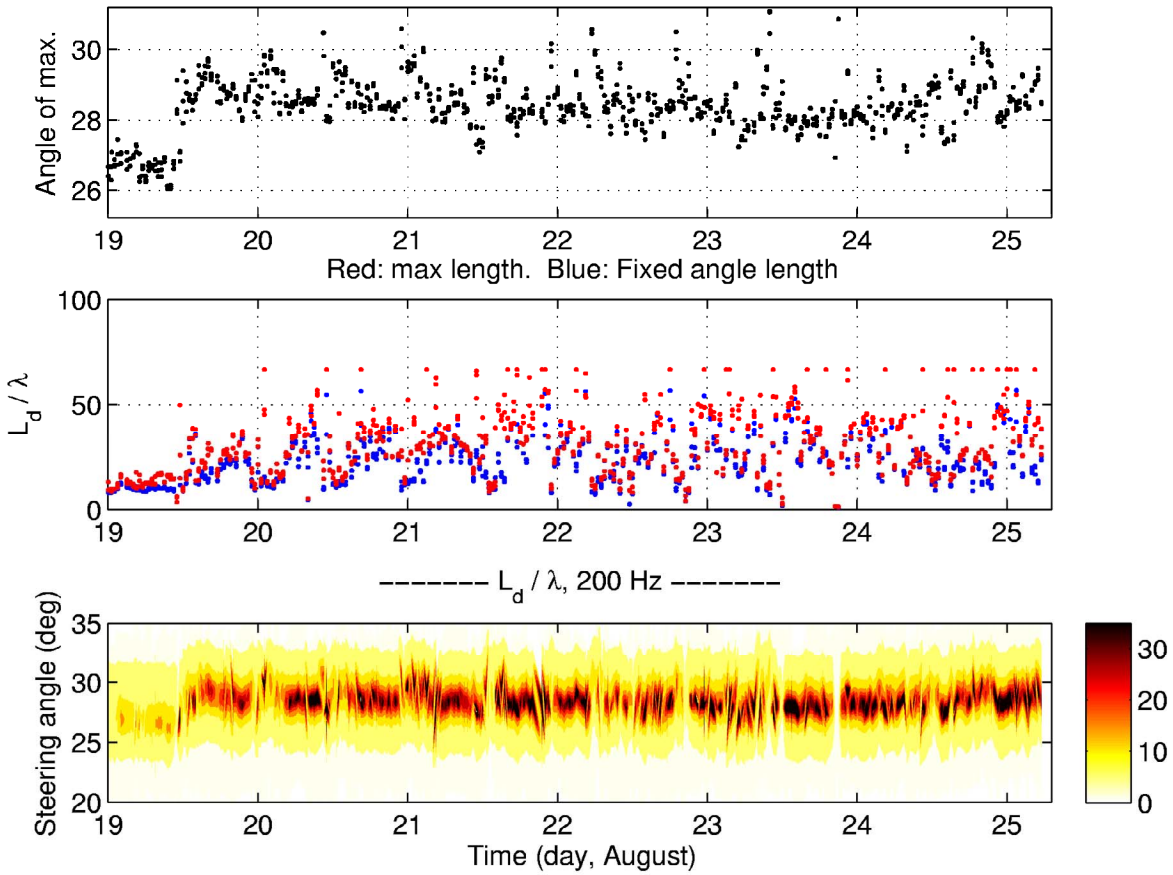

Figure 4. Pulse parameters for the 200-Hz northeast source are shown. These computations use the array shape determined for the period after 1000 UTC August 19. (bottom) The coherence length is contoured versus steering angle and time (six days). (center) The red dots show the maximum coherence length as a function of time. The blue dots show the coherence length a the fixed angle of 28.2 degrees. (top) The angle of maximum coherence is plotted.

[(bottom) Fluctuating angle of peak coherence and peak coherence level is seen. (center) The peak and fixed-angle correlation values (often the same) are seen to (roughly) oscillate at a two-per day period, a major periodicity of the tidally generated internal wave packets. The coherence length varied between 5 and 50 wavelengths. (top) The angle (direction) of maximum coherence oscillates between 28 and 30 degrees during the three days of most active waves.]

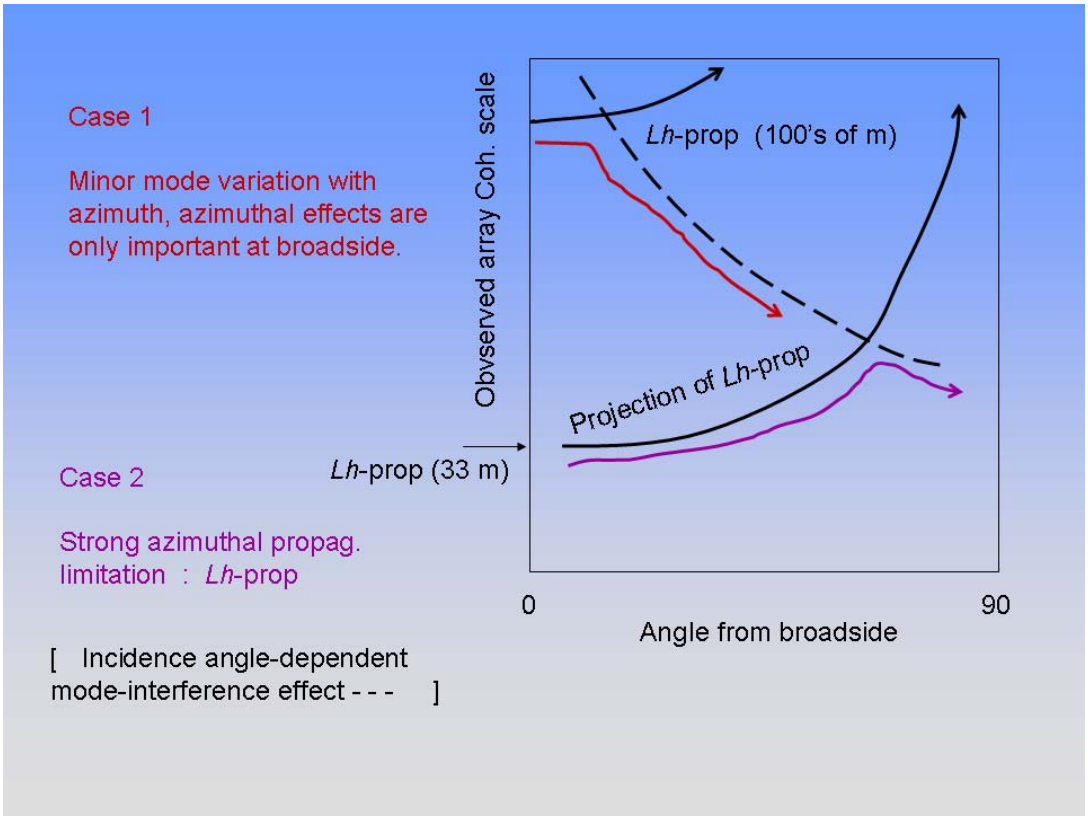

Figure 5. Interpretation of two coherence length situations observed in the 100 and 200-Hz pulse data received at the L-array. The red line (Case 1) corresponds to the long coherence scale case, where interference governs correlation in the experimental situation of 63 degrees from broadside. The lavender line (Case 2) corresponds to the short-coherence scale case, where the coherence at this angle is governed not by ubiquitous mode interference (dashed line), but by decorrelation processes with azimuthal dependence as measured from the source position. Note that the "projection of L_h-propagation" lines rise as $1/\cos\theta$, where θ is angle from broadside.

[As pulse arrival angle from broadside moves from zero to 90 degrees, the red Case-1 line drops. It is near the dashed line for true plane-wave mode arrivals everywhere except at broadside, where it is lower then the dashed line because of weak departure from plane wave geometry (weak azimuthal variability). The lavender Case-2 line starts low at angle zero (broadside) and rises because of a geometric effect until it intersects the dashed line at an angle between 45 and 90 degrees.]

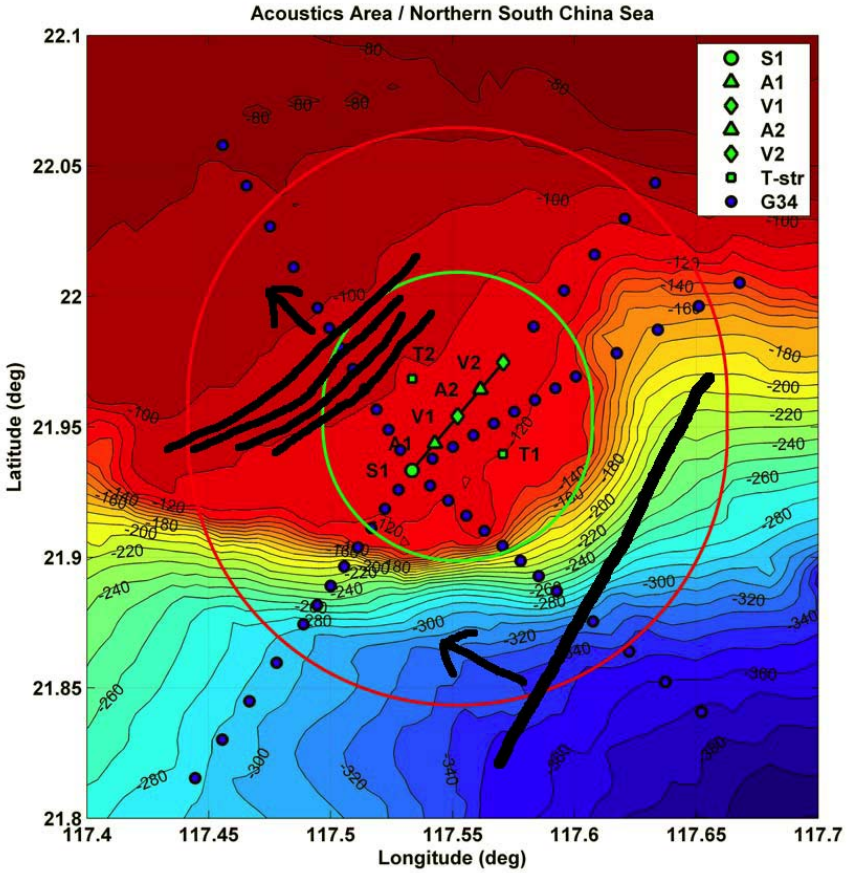

Figure 6. Bathymetric chart showing the 2007 NLIWI experiment area. Eight moorings were placed, shown in green. Five are along the acoustic propagation line: S1, 400-Hz acoustic source; A1 (ADCP) 1.48 km from S1; V1 (VLA) 3.00 km from S1; A2 (ADCP) 4.43 km from S1; and V2 (VLA) 6.01 km from S1. The heading along the mooring line is 40° True. Three additional thermometer array moorings were: T1, 2.45 km @ 130° from V1; T2, 2.50 km @ 310° from V1, and T3, 6.66 km @ 322° from V1. The blue dots show intended dipped acoustic source stations. The black lines schematically depict, at the right, an incident internal wave of depression and at the left a packet of waves on the shelf of the type formed from such waves.

[The A1 to V2 mooring line (acoustic propagation line) is approximately parallel to the crests of nonlinear internal waves arriving from the east.]

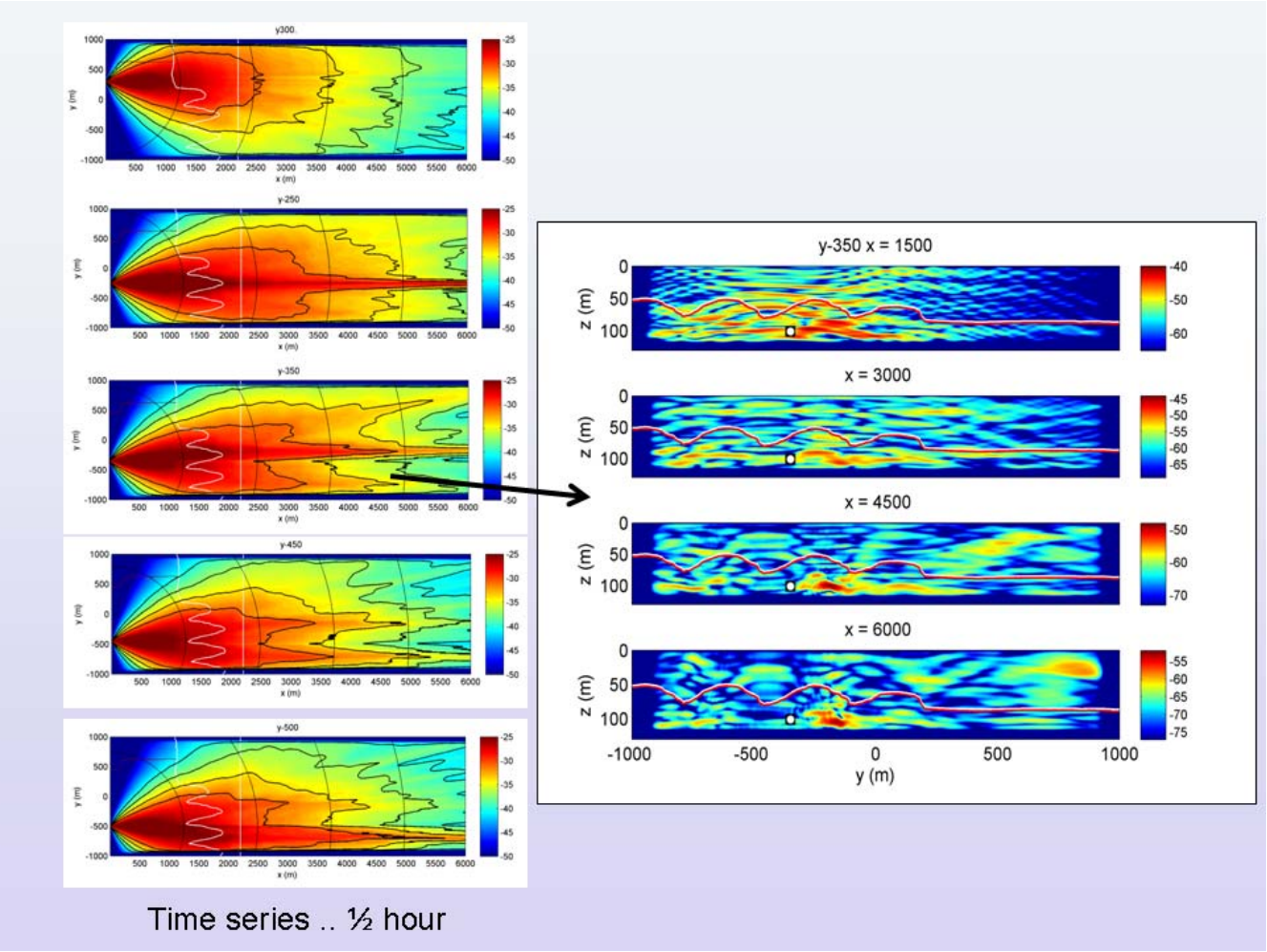

Figure 7. 3D-PE Modeling of SCS 2007 experiment. On the left are panels showing plan views of depth-averaged sound field from source at five positions relative to a group of passing internal wave with shape extracted from the data set. The source positions of high-intensity sound (indicated by red) are at x=0 and various y. The seafloor is flat here, so the model runs simulate a time series. When the source is located between waves of elevation there is strong ducting, as observed in the experiment. Some of the rums show beams at angles not parallel to the waves, which have uniform crests running across the page left to right. On the right are panels showing sound intensity in the y-z plane at four different ranges (x) for one source position. The internal wave that is independent of x is shown in each panel.
[The internal waves duct sound such that intensity can increase by 10 dB at 6 km maximum range. The panels at right show high intensity in an internal wave duct containing the source.]

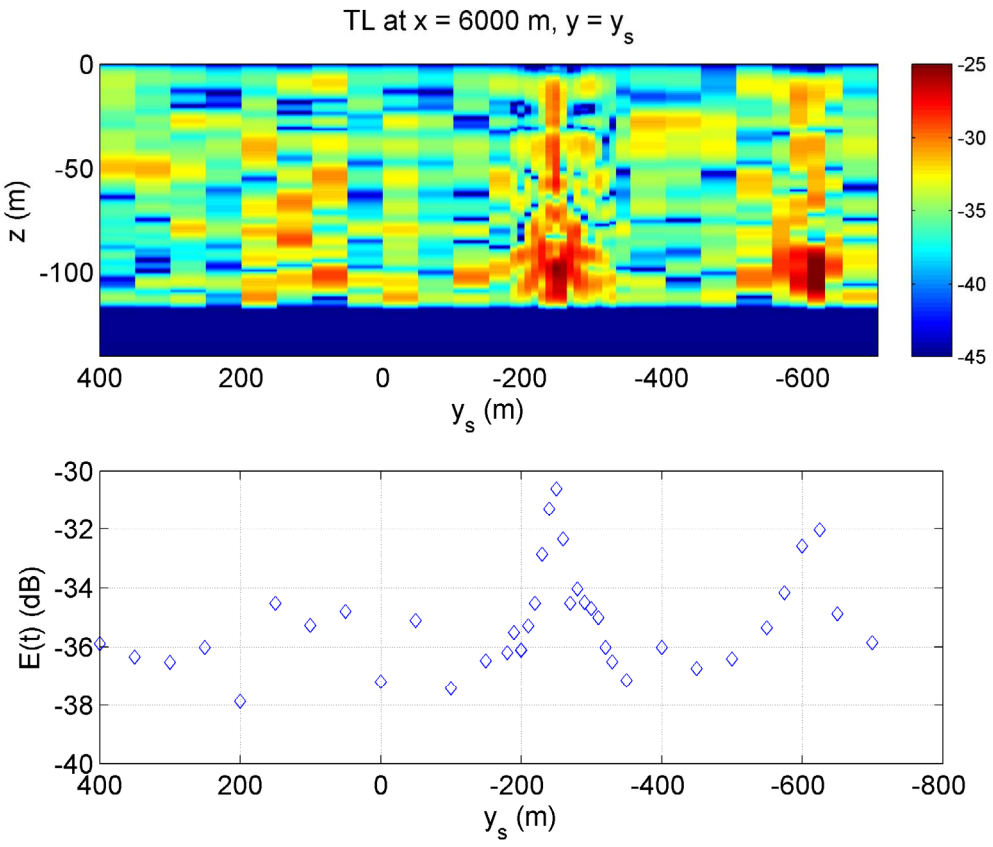

Figure 8. Acoustic field properties from thirty 400-Hz 3D simulations are shown. For variable source position ys and fixed wave position (as shown in Figure 7) the top panel shows transmission loss (intensity) at y = ys and x = 6000 m. This sound had propagated parallel with the wave ducts. The lower panel shows depth-mean intensity at the same location. The horizontal axis is reversed so that a time series for a wave passing by a fixed source/ receiver geometry is imitated. Based on the wave speed observed in the field the figure shows approx. ½ hour of time.

[Panels show about a 7 dB increase in depth averaged intensity when both the source and receiver are in a single duct (ys of about -230 and -610 m) as compared to intensity when they are not both positioned in a connecting duct.]